IJCRT.ORG ISSN : 2320-2882

INTERNATIONAL JOURNAL OF CREATIVE RESEARCH THOUGHTS (IJCRT)

An International Open Access, Peer-reviewed, Refereed Journal

Potable water production from surrounding air

Dr. Eng. Mohammed Alsheekh [1] **Ass. Prof. Dr.** Hussein S. Sultan [2]

[1, 2] Department of Mechanical Engineering, Engineering College, University of Basrah, Al Basrah, Iraq.

Abstract: The prevention of coronavirus outbreaks requires cleaning and refreshing the closed environment where people live and operate. As a result, new environmental control methods must be developed. Also, water shortages represent an urgent problem, mainly countries that are island states and countries that have long coastlines which don't have sufficient water resources such as lakes and rivers. This paper is an experimental, theoretical and numerical study of air purification and water generation by air conditioning and refrigeration equipment. The unit is based on a standard compressive cooling cycle principle. The experimental device will be established and tested in Basra city, south of Iraq, during September and August from 2020. The experimental device was tested for different days with different climatic conditions. Theoretical data has been completed by the (EES) program and the Numerical study by (ANSYS 2020R2) to verify and study more cases in a short time with no cost. The maximum production rate is 45.7 L/Day with the system's performance factor of COP Max=4.0, Min=2.3, and aver. =3.4. Therefore, the device can be used in coastal areas to meet water needs and provide a healthy environment.

1. Introduction

One of the pressing challenges in today's world is the lack of potable water. Although water covers more than two-thirds of the earth's surface, potable water used for drinking is scarce. Countries with island states and long coastlines that don't have adequate freshwater resources, such as lakes and rivers, face an acute water shortage. As a result, most of these countries get their water by desalinating seawater, a very costly solution. Similarly, desalination plants can fail. Therefore, alternative ways to produce water are urgently required to meet their water production needs. Many coastal areas have relatively high humidity (about 70-90 percent). Thus, with a dehumidifying device, gathering water from the air can meet the water needs for many people. **[1]. Habeebullah (2009) [2]** designed a chart for rapid prediction of water efficiency using any combination of ambient air temperature (25°C < Ta < 40°C) and relative humidity (30% < RH < 100%). Water yield due to air dehumidification was calculated using a model designed to compare surface efficiency with moist air transition. The daily variance in water yield (Jeddah/Saudi Arabia) showed that the relative humidity pattern was held to a minimum at midday. Maximum water yield was forecast for August (17.6 kg/m2/ day) at (2.25 m/s) air velocity. The average estimated water yield in August and February was (509 and 401 kg/m2). **Bogardi et al. (2012) [3]** investigated and showed that sustainability, fair distribution, and conservation of water resources must occur within integrated water management and governance, but implementation is problematic. Continuing global climate change, growing population, urbanization, and striving for better living conditions poses a challenge to planetary sustainability. **Magrini et al. (2015) [4]** studied A range of technologies to learn how to extract water from the atmosphere. New equipment can remove both water and air from the same evaporator. This (HVAC) system is being used in a dry, hot environment for demonstration purposes. Traditional (HVAC) systems and integrated AC systems should be compared in this way. **Tripathi et al. (2016) [5]** studied atmospheric water generation (AWG) under the same rules as refrigerators and climate control. This worked by changing barometric air pressure by pressurizing the air using a compressor and then passing the air through condenser pipes, decreasing the temperature to the dew point. **Bagheri (2018) [6]** investigated experimentally the performance and limitations of commercially available air water harvesting (AWH) systems. Results show the range of water harvesting rates and energy intensity varying from (1.02 kWh/L) for warm and humid to (6.23 kWh/L) for warm and humid climates. **Fares Mohamad et al. (2019) [7]** studied and designed a model of water desalination that works with HDH technology and has obtained a production of 1.71 kg/hr with a consumption capacity of 726 watts. Therefore, there has been a conclusion that these small units are a reliable way to desalinate water.

This study aims to construct, test, and simulate atmospheric water generation devices. The device will condense the water vapor in the atmosphere and purify it to be suitable for human use. The requirements are identified to ensure that the research effectively fulfils its intended purpose. First, this design's possibility of using water for drinking

products must be compatible with the (WHO) drinking water quality standards. The design of this product should be simple enough for users with limited technical experience. Finally, the design should be safe enough not to harm users during regular operation. By changing the way, the usual air conditioning cycle is made, it can be used for more than one thing. For example, it can make water from the air, clean and condition the air while it is being filtered and heated, and work as both an external and an internal air conditioner.

2. Experimental device

2.1. Components used

The components used for the construction of the water generation device are shown below in Table 1.

Table 1. Shows Details of Components of System Model.

Item	Component name	Quantity	Specification
1	Compressor	1	220V50HZ AC, 2.1 KW, 18000BTU
2	Condenser	1	Area 42cmx42cm, N_{pipe}=20, Copper 1/2 ".
3	Evaporator	1	Area 42cmx84cm, N_{pipe}=40, Copper 1/2 ".
4	pipes	Set	Copper coated fins
5	Control system	Set	220 V AC + Transformer 12V DC+ wiring
6	Fan	1	Centrifugal fan, constant velocity
7	Plastic Glass with all accessories	Set	Insulated plastic
8	Osmosis filtration system	Set	Seven stages filtration (RO)
9	Air filters	2	One to evaporator and another for condenser

2.2 . Description

A multi-purpose device (water generation, air cleaning, and air conditioning). It is designed, and it consists of the following parts:

1- The hot section of this system is located in an isolated and separate room that includes a compressor, hot tubes, and condenser.
2- The cold section includes an evaporator, capillary tube, and cooling tubes located in an isolated and separate room.
3- A central fan to draw air from both hot and cold sides and discharges it to the required regions.
a- In the cold section, the air is passed through the evaporator tubes and discharge to a select region.
b- In the hot section, the air is passed through the condenser tubes and then discharged to the atmosphere.
4- Copper tubes are used for both the condenser and the evaporator. Fins surround the tubes along their length to increase the surface area and increase the heat exchange rate.

The constructed device in this study will perform the following tasks:

1- Generating water from the air.
2- Purification and conditioning of the atmosphere during its filtering and thermal treatment. The device's details will be shown in figures number 1, 2, 3, and 4.

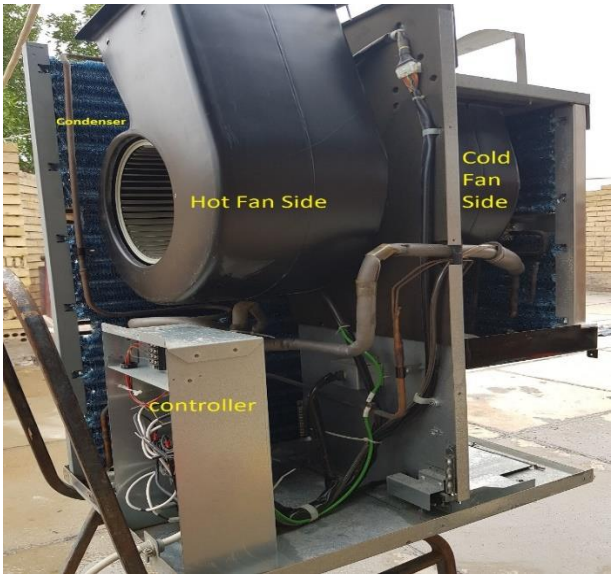

Figure 1. Elements of system No.1.

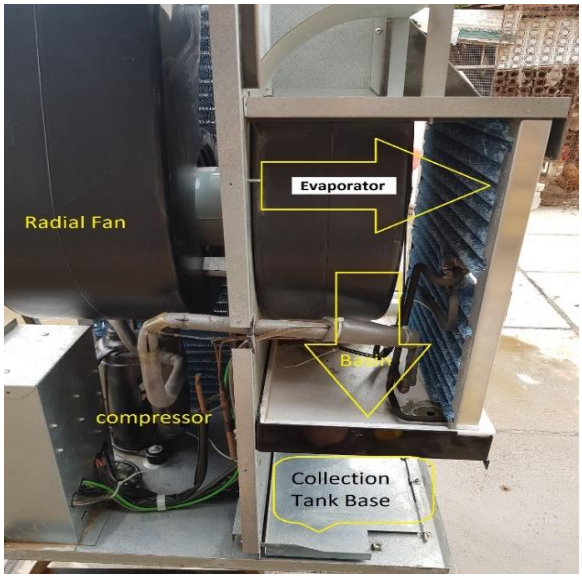

Figure 2. Components of system No.2.

Figure 3. Details of Filtration system.

Figure 4. Actual picture during system activities.

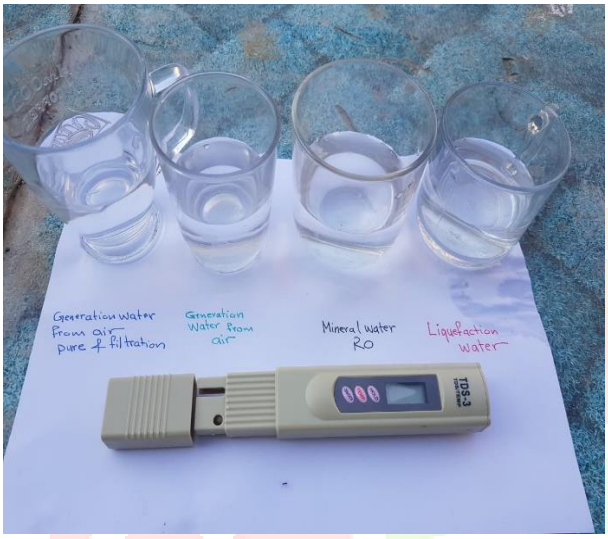

Figure 5. Different water to test.

Figure 6. Actual photos during testing.

3. Measuring instruments

The measuring devices used during the experiments are Anemometer-Psychometric, infrared thermometer, temperature-humidity meter, and TDS-tester, shown in Figure 7.

infrared thermometer

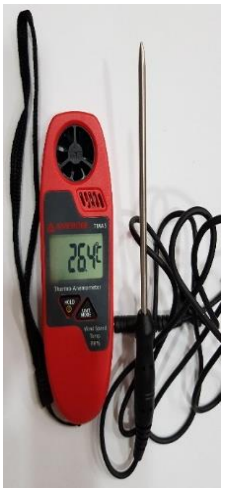

Anemometer-Psychometric

temperature-humidity meter

temperature-humidity meter

TDS tester

Figure 7. Measuring instruments.

4. Theoretical analysis

4.1. vapor compression cycle

The vapor compression cycle explained below is the most common type of system used in refrigeration and air conditioning. **[8]**

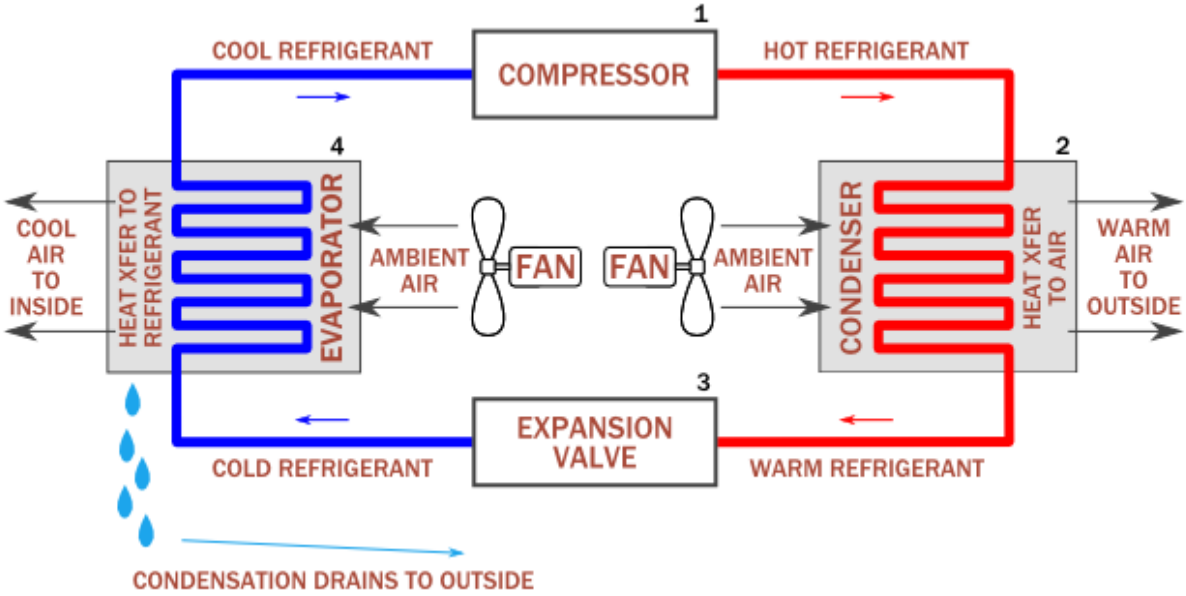

Figure 8. Diagram of refrigeration vapor compression cycle.

4.2. C.O. P Carnot cycle & C.O.P Actual cycle

The standard of comparison for the performance of the refrigeration cycle is the coefficient of performance (COP) of the Carnot refrigeration cycle, which is given by the following equation: **[9]**

$$COP_{R,carnot} = \frac{(273+T_c)}{(T_h - T_c)} \qquad (1)$$

The COP of the actual cycle is the rate of heat absorbed in the evaporator (Q) and the work (W) required for the compressor, which is calculated from the experimental data as follows:

$$COP_{R,actual} = \frac{cooling\ effect}{work\ input} = \frac{heat\ absorbed}{(heat\ rejected - heat\ absorbed)} = \frac{Q}{W} \qquad (2)$$

4.3. Theoretical Prediction of Available Water Vapor in The Air

The air contains water vapor in varying amounts. In the desert, the air is dehydrated, and in tropical jungles, it is very moist. As a result, the water vapor in the air is in the form of a super-heated state. Therefore, both dry air and water vapor are assumed to behave like a perfect gas.

The ratio of (m_v/m_a) is defined as humidity ratio denoted by the term (W_s), which is "the mass of Vapor associated with one Kg of dry air," also known as mixing ratio or moisture content. When (t_d) is the saturation temperature, and the partial pressure of air is P_s, the humidity ratio for saturated air is given:

$$W_s = 0.622\ \frac{P_s}{(P_b - P_s)} = \frac{Kg}{kg\ of\ dry\ air} \qquad (3)$$

for humid air is given by:

$$W = 0.622\ \frac{P_w}{(P_b - P_w)} = \frac{Kg}{kg\ of\ dry\ air} \qquad (4)$$

Where:

W_s = moisture required to saturate 1 Kg of dry air.

P_s = saturated pressure of vapor corresponding to dry bulb temperature from steam table **[12]**.

P_w = partial pressure of water vapor.

P_b= barometric pressure.

5. Simulation using The ANSYS 2020R2 (CFD) code

The numerical simulation of the experimental device is performed using the ANSYS 2020R2 software. The solution of time-averaged conservation equations of mass, momentum, energy, and species in steady three-dimensional flows using finite volume is applied. The vector form of the governing equations is:

$$\frac{\partial}{\partial t}(\rho\emptyset) + div\{(\rho v\emptyset)\ - (\Gamma_\emptyset grad_\emptyset)\} = S_\emptyset \qquad (5)$$

Where: ρ, v, $\Gamma_\emptyset$, and $S_\emptyset$ are density, velocity vector, effective exchange coefficient of $\emptyset$, and source rate per Unit volume, respectively, for a solved-for variable $\emptyset$. The discretization of the domain is followed by reducing the previous equations to their finite domain form using the coefficients' hybrid formulation. The solution technique employs the SIMPLEST algorithm (an improved version of the well-known SIMPLE algorithm). The standard ***(k-ε)*** turbulence model is applied. **[10]** The general steps for the ANSYS simulation are given in **Table 3.**

Table 3. Shows the General Steps for The Ansys Simulation.

Steps	Item	Description
1	Geometry **Figures 9,10.**	First, the model is imported to ANSYS2020-R2 workbench from design modular with the following specifications. The dimensions of the inlet side were 42 x42 cm, the air outlet duct was 42 x 42 cm, and the evaporator was 42 x 42 cm, and this was used for 20 pipes.
2	Mesh quality Figure 11.	Minimum orthogonal quality = 3.62012e-01 cell 106049 on zone 6 (ID: 106050 on partition: 0) at location (1.45788e-01 4.52793e-02 4.95000e-01) Maximum aspect ratio = 1.87973e+01 cell 107351 on zone 6 (ID: 107352 on partition: 0) at location (2.58259e-02 3.26994e-02 1.50000e-02).
3	Setup **Figure 12.**	Included Fluent launcher, general, models, materials selection, air properties, boundary conditions, reference values, solution methods, solution initialization, run calculation, and solution convergence.
4	Results	Included ANSYS CFD post as results for inlet temperatures, outlet temperatures, different velocities, and humidity.

6. Results and Discussion and Conclusions

6.1 Boundary Conditions

The boundary conditions applied for the numerical simulation by the Ansys fluent 2020 are given in **Table 4.**

Table 4. Shows the boundary conditions for fluent simulation.

No.	Boundary Conditions	Details
1	Inlet B.C. (Momentum)	Four different values of mean axial supply X-velocity are studied, which are (0.25 m/s, 0.5 m/s, 0.75 m/s, 1.2 m/s) and turbulence intensity of 5%
2	Inlet B.C. (Thermal)	Eight values for inlet air temperature are studied, which are (287K, 293K, 298K, 303K, 308K, 313K, and 318K)
3	Outlet B.C.	Gauge pressure (pascal)
4	Wall B.C.	Stationary wall and no-slip and adiabatic
5	The cover B.C.	Adiabatic wall

6.2 Results and Discussion

August and September from 2020. The experiment was designed to take 24 readings in 60 days. The time required for each reading ranged from a minimum of 6 hours to a maximum of 24 hours. During the experimental day, the variation of the dry bulb temperature ranged from 25℃ to 48℃, and the relative humidity ranged from 10% to 100%. The theoretical (case2) prediction for the variation of water vapor content in the air for different DBT and RH was also given to verify and compare it with experimental results. Finally, (case3), the simulation using ANSYS 2020 is performed.

6.2.1. Case 1 (Experimental Case)

Actual operation tests for the water generation device were performed for two months in 2020 (from 01-08-2020 to 30-09-2020). The relative humidity range was between (10% -100%), and the temperatures recorded were between 25℃ and 48℃. The water generated was collected every hour with different DBT, DPT, and RH, which can be seen in **Tables 5 and 6**. **Table 7** has the summation of the collected water for all hours of operation that represents the amount of water and the corresponding average daily temperatures and relative humidity that were recorded. The range of water production rate for the experiments held in August and September of 2020 was from (4.3 L/day to 45.7 L/day), which is suitable for the size of the experimental device in these conditions.

Humidity in the air is varied with time, and the conditions were not even similar, so the amount of water produced was not constant. The variation of water production rate with relative humidity and temperature will be shown below in **Table 7** and **Chart 3**. The water production depends on three factors: DBT, DPT, and RH, which can be shown by the amount of water produced.

The results viewed in the **Tables 5 and 6** are for two days, the first day was on 18-8-2020, representing the minimum production rate, and the second was on 6-9-2020 and represented the maximum production rate.

From **Table 5** and **Chart 1** it can be seen that the test on 18-08-2020 has the lowest water production rate during August. The device operated for the full day, and the results obtained were shown in the table below, where the temperature behavior and the effect on the water production rate are discussed. The effects of the dew point and the decreasing humidity were also explained. The decrease in humidity and rising temperature dropped the moisture level, which then affects water production. The water production rate decreased with decreasing humidity with little change in dry bulb temperature from (12:00 AM to 09:00 AM). **Chart 1** represents the relationship between DBT, DPT, RH, and the amount of water produced. The water production rate increased between 12 AM to 6 AM when DBT and DP decreased and RH increased. This means that the water production rate is inversely proportional to a rising temperature and directly proportional to a rising RH.

From **Table 6 and Chart 2** it can be seen that the test on 06-09-2020 has the highest water production rate during September. The water production rate increased from 12 AM to 8 AM when the RH increased with very little increase in temperature. After this period, the humidity decreases, and the temperature increases, which causes the water produced to decrease during the period between 1 PM and 6 PM. The production rate of water increase as humidity rises, and the temperature decrease from 7 PM to 11 PM. The water production rate increased from 0.3 to 3.8 L/h when the humidity increased with the temperature range of 29℃ to 44℃. This means that RH variation has a more significant effect on the water production rate than the variation in dry bulb temperature.

Table 7 and Chart 3 show that the water production rate correlates with the average dry bulb temperature and average relative humidity. Also, the water production rate for the average relative humidity increased with the increasing dry bulb temperature during the two months' tests. Also, increasing the hours of operation led to an increased water production rate. That means the water production rate increased with an increase in average humidity in the range of the average temperatures recorded, all dependent on operation hours.

Table 8 represents a comparison between COP of Carnot with COP of actual cycle. The maximum, minimum, and average COP for the actual cycle was (C.O.P Max=4.0, Min=2.3, Aver=3.4). While the COP of Carnot is more than twice as accurate as the COP of the actual cycle because the Carnot is an ideal performance factor, so the actual calculation is a suitable value for this module.

Table 5. The amount of water present at different temperatures and different RH according to production hours.

Date of Day	Time (h)	DB Temp.	Dew Point	Relative Humidity RH %	Amount of water L/h
18/08/2020	12:30 AM	32	11	28	0.4
	1:30 AM	32	10	27	0.3
	2:30 AM	31	11	29	0.4
	3:30 AM	30	10	30	0.4
	4:30 AM	29	10	31	0.4
	5:30 AM	29	10	31	0.4
	6:30 AM	28	9	31	0.4
	7:30 AM	31	8	25	0.3
	8:30 AM	35	8	21	0.2
	9:30 AM	37	8	18	0.0
	10:30 AM	40	7	16	0.0
	11:30 AM	42	6	14	0.0
	12:30 PM	44	4	13	0.0
	1:30 PM	45	4	11	0.0
	2:30 PM	45	4	11	0.0
	3:30 PM	46	3	11	0.0
	4:30 PM	45	3	11	0.0
	5:30 PM	44	5	12	0.0
	6:30 PM	42	5	13	0.0
	7:30 PM	39	8	17	0.0
	8:30 PM	37	8	19	0.2
	9:30 PM	36	10	22	0.3
	10:30 PM	34	11	25	0.3
	11:30 PM	33	12	28	0.4
		36.91667	**7.708333**	**20.58333**	**4.3**
		average	**average**	**average**	**L/Day**

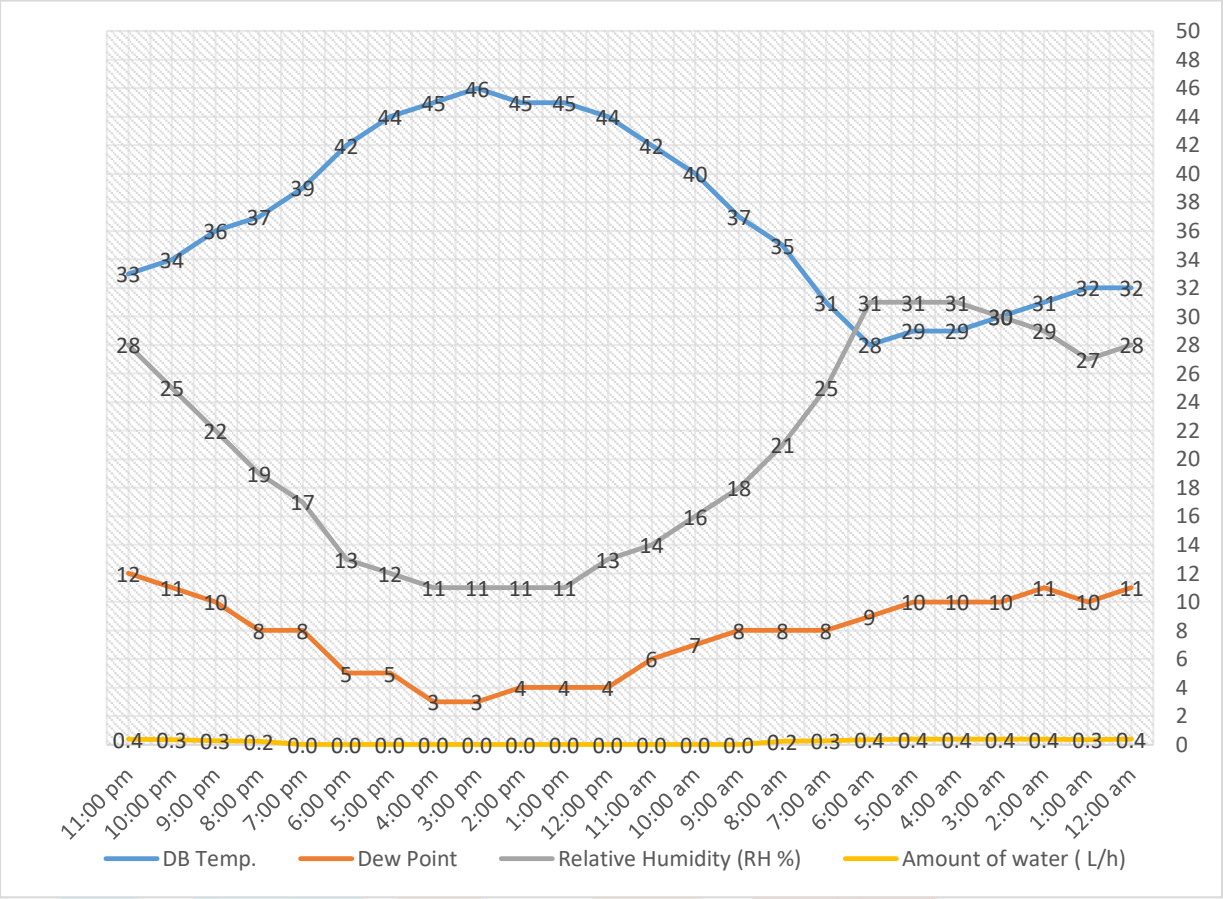

Chart 1. The amount of water present at different conditions through one day.

Table 6. The amount of water present at different temperatures and different RH according to production hours.

Date of Day	Time (h)	DB Temp.	Dew Point	Relative Humidity (RH %)	Amount of water (L/h)
06/09/2020	12:30 AM	29	28	85	2.9
	1:30 AM	28	29	95	3.5
	2:30 AM	28	29	97	3.6
	3:30 AM	27	29	100	3.6
	4:30 AM	27	28	99	3.6
	5:30 AM	27	29	98	3.5
	6:30 AM	27	29	98	3.5
	7:30 AM	29	31	97	3.8
	8:30 AM	32	29	82	3.3
	9:30 AM	35	29	65	2.4
	10:30 AM	39	26	47	1.6
	11:30 AM	41	21	36	1.0
	12:30 PM	43	18	26	0.6
	1:30 PM	44	14	19	0.3
	2:30 PM	45	12	17	0.3
	3:30 PM	45	11	16	0.2
	4:30 PM	44	11	16	0.2
	5:30 PM	43	12	19	0.3
	6:30 PM	40	17	27	0.5
	7:30 PM	36	19	37	0.8
	8:30 PM	34	21	46	1.1
	9:30 PM	33	23	54	1.5
	10:30 PM	31	23	61	1.7
	11:30 PM	30	25	67	1.9
		34.875	**22.625**	**58.5**	**45.7**

	Average	Average	Average	L/Day

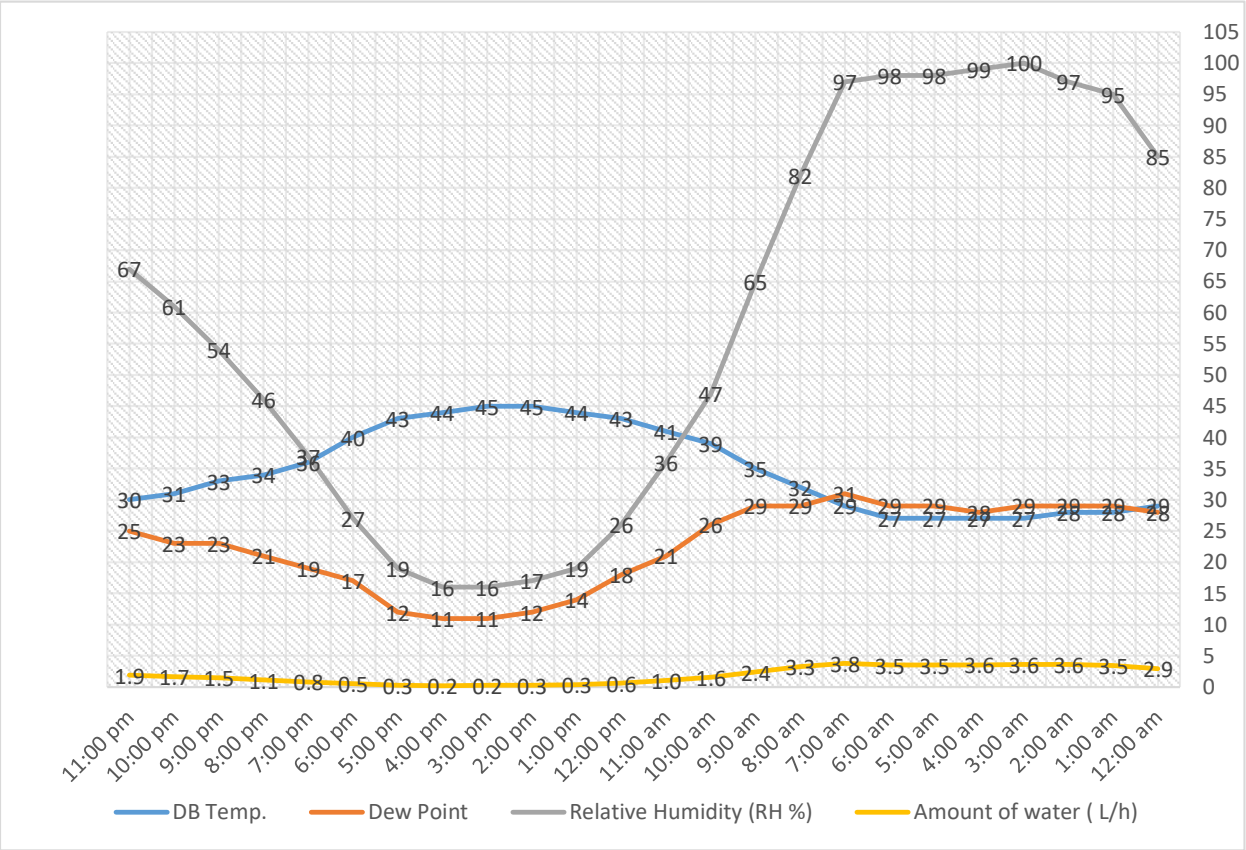

Chart 2. The amount of water present at different conditions through one day.

Table 7. The amount of water present at different temperatures and different RH according to production Days.

N0.	Day	Active Hour	Average EXP. DBT (C)	Average EXP. DPT (C)	Average EXP. RH (%)	Amount of production for one day (L/Day)
1	15/08/2020	18	38.2	14.1	36.5	16.4
2	16/08/2020	16	36.6	9.3	25.5	4.9
3	17/08/2020	12	35.6	8.6	24.9	4.9
4	18/08/2020	24	36.9	7.7	20.6	4.3
5	19/08/2020	12	36.1	8.9	23.2	3.2
6	20/08/2020	12	36.3	9.4	23.6	3.5
7	21/08/2020	14	36.4	9.3	24.8	4.3
8	22/08/2020	13	36.6	9.7	22.6	3.0
9	23/08/2020	15	36.8	13.1	29.8	8.5
10	24/08/2020	14	37.2	12.7	28.3	7.6
11	25/08/2020	9	36.9	9.5	22.7	3.2
12	26/08/2020	18	35.7	8.6	21.8	2.2
13	27/08/2020	16	35.3	7.9	21.8	2.1
14	28/08/2020	12	35.6	7.7	22.8	2.7
15	29/08/2020	9	36.0	8.3	22.2	2.5
16	30/08/2020	12	36.0	9.9	24.0	3.6
17	31/08/2020	16	36.0	15.0	32.7	10.5
18	01/09/2020	18	36.0	20.2	49.2	27.9
19	02/09/2020	18	36.2	18.7	45.9	25.3
20	03/09/2020	15	37.5	12.2	26.6	6.2
21	04/09/2020	13	36.5	14.3	31.8	11.1
22	05/09/2020	24	34.8	22.8	58.1	39.3

23	06/09/2020	24	34.9	22.6	59.0	45.7
24	07/09/2020	18	35.5	16.3	46.0	24.3
25	08/09/2020	12	37.3	8.9	21.1	2.4
26	09/09/2020	11	37.0	8.9	23.0	3.4
27	10/09/2020	14	36.3	11.1	27.0	5.8
28	11/09/2020	13	36.2	9.2	23.6	3.3
29	12/09/2020	11	36.1	8.8	23.5	3.2
30	13/09/2020	12	35.8	8.5	23.3	3.0
31	14/09/2020	15	35.6	10.0	25.3	4.3
32	15/09/2020	14	35.4	11.9	25.5	4.7

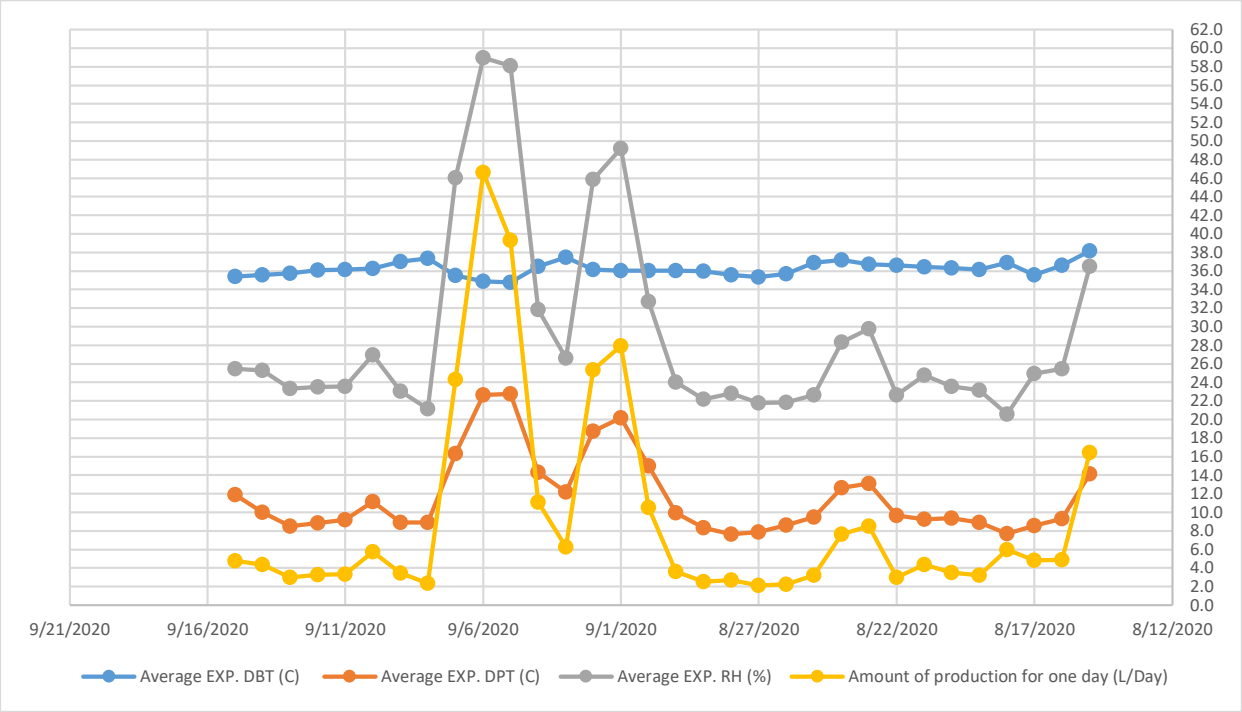

Chart 3. The amount of water present at different temperatures and different RH according to production Days.

Table 8. Represent comparison between COP $_{Carnot}$ with COP $_{actual}$

Date	Time	T1	T2	Condenser Pipes Temp	Evaporate Pipes Temp	COP Carnot	Q	COP actual
21/09/2020	09:19 PM	36	11.8	41.4	7.2	8.2	7.3	3.5
22/09/2020	12:28 pm	42	14.9	44.2	10.1	8.3	8.2	3.9
22/09/2020	04:55 pm	43.8	14.9	45.8	11.1	8.2	8.7	4.1
22/09/2020	08:08 pm	34.4	12.2	41.5	8.8	8.6	6.7	3.2
22/09/2020	09:56 pm	33.9	10.8	40.9	6.3	8.1	7.0	3.3
23/09/2020	8:00 am	33.1	11.5	38.7	7.4	9.0	6.5	3.1
23/09/2020	11:09 am	41	13.4	39	8.3	9.2	8.3	4.0
23/09/2020	7:26 pm	36.4	13.1	38	9.1	9.8	7.0	3.3
23/09/2020	9:49 pm	35.6	12.4	39.6	8.7	9.1	7.0	3.3
24/09/2020	4:09 pm	43.2	16.1	50.3	10.7	7.2	8.2	3.9
24/09/2020	8:00 pm	34.1	13.3	42.7	9.4	8.5	6.3	3.0
24/09/2020	10:17 pm	32.1	13	40.5	9.7	9.2	5.8	2.7
24/09/2020	11:08 pm	34.7	13	40.1	9.5	9.2	6.5	3.1
25/09/2020	11:26 am	40.3	14	46.2	8.6	7.5	7.9	3.8
25/09/2020	8:28 pm	33.5	13.3	42.9	9.6	8.5	6.1	2.9
25/09/2020	9:55 pm	34	13.5	41.1	10.6	9.3	6.2	2.9
25/09/2020	11:53 pm	32.1	13.1	41	9.7	9.0	5.7	2.7
26/09/2020	9:34 am	36.5	11.8	42.1	7.3	8.1	7.4	3.5

26/09/2020	1:51 pm	42.1	14.4	48.5	8.6	7.1	8.4	4.0
26/09/2020	7:08 pm	36	13.1	45.5	8.1	7.5	6.9	3.3
26/09/2020	9:48 pm	31.7	12	43.1	7.3	7.8	5.9	2.8
						8.4		**3.4**

6.2.2. Case 2 (Theoretical Case)

A mathematical calculation was used to get to the Saturation Pressure point (PS). The saturation pressure of water at different atmospheric temperatures is obtained from available steam tables. Air is a mixture of both dry air molecules and water vapor molecules. The partial pressure of water (PW) is the water vapor pressure present in a mixture of air and water vapor. The (RH) is the ratio of the partial pressure of water (PW) to saturation pressure (PS).

In chart 4 the x-axis represents temperatures, and the amount of water produced is the y-axis, while the curves represent the percentage of relative humidity. The amount of water produced in L/day in the curve increases with RH increases, similar to our experimental calculation.

Theoretical predictions for the dew point temperature, the percentage of moisture, and the amount of water in the cubic meter of the air have been calculated. The calculations are performed for different relative humidity and dry bulb temperature values in the range of (10%-100%) and (15℃ - 50℃). The results in **Table 9** are for RH of 35% and 100%, and the temperature is varied from (25℃ - 45℃), while **Chart 4** represents all results. The theoretical predictions are consistent with the experimental results. The behavior is the same as that of the experimental results for increasing the water production with increasing the relative humidity and dry bulb temperature.

Table 9. The amount of water present (1m3) in different temperatures and different RH.

Temp	Saturation Pressure P_s (bar)	Relative Humidity (RH %)	Partial Pressure of water-P_w (bar)	Humidity Ratio	Amount of water (L/m^3 air)
25	0.032	35	0.0112	0.006952148	6.9521481
26	0.034	35	0.0119	0.007391821	7.391821
27	0.036	35	0.0126	0.007832109	7.8321091
28	0.038	35	0.0133	0.008273014	8.2730137
29	0.04	35	0.014	0.008714536	8.7145359
30	0.042	35	0.0147	0.009156677	9.1566772
31	0.045	35	0.01575	0.009821053	9.8210526
32	0.048	35	0.0168	0.010486828	10.486828
33	0.05	35	0.0175	0.010931459	10.931459
34	0.053	35	0.01855	0.011599578	11.599578
35	0.056	35	0.0196	0.012269109	12.269109
36	0.059	35	0.02065	0.012940056	12.940056
37	0.063	35	0.02205	0.013836864	13.836864
38	0.066	35	0.0231	0.014511135	14.511135
39	0.07	35	0.0245	0.015412389	15.412389
40	0.074	35	0.0259	0.0163162	16.3162
41	0.078	35	0.0273	0.017222577	17.222577
42	0.082	35	0.0287	0.018131532	18.131532
43	0.087	35	0.03045	0.019271368	19.271368
44	0.091	35	0.03185	0.020186163	20.186163
45	0.096	35	0.0336	0.021333333	21.333333
Temp	**Saturation Pressure Ps (bar)**	**Relative Humidity (RH %)**	**Partial Pressure of water-Pw (bar)**	**Humidity Ratio**	**Amount of water (L/m^3 air)**
25	0.032	100	0.032	0.020284331	20.2843312

26	0.034	100	0.034	0.021596119	21.5961195
27	0.036	100	0.036	0.022913277	22.9132771
28	0.038	100	0.038	0.024235837	24.235837
29	0.04	100	0.04	0.025563833	25.5638325
30	0.042	100	0.042	0.026897297	26.8972973
31	0.045	100	0.045	0.028907823	28.9078234
32	0.048	100	0.048	0.030930847	30.9308469
33	0.05	100	0.05	0.03228653	32.28653
34	0.053	100	0.053	0.034330643	34.3306431
35	0.056	100	0.056	0.036387569	36.3875686
36	0.059	100	0.059	0.038457427	38.4574273
37	0.063	100	0.063	0.041237569	41.2375691
38	0.066	100	0.066	0.043338084	43.3380839
39	0.07	100	0.07	0.046159555	46.1595547
40	0.074	100	0.074	0.049005057	49.0050572
41	0.078	100	0.078	0.0518749	51.8748998
42	0.082	100	0.082	0.054769396	54.769396
43	0.087	100	0.087	0.058422672	58.4226721
44	0.091	100	0.091	0.061373814	61.373814
45	0.096	100	0.096	0.065098937	65.098937

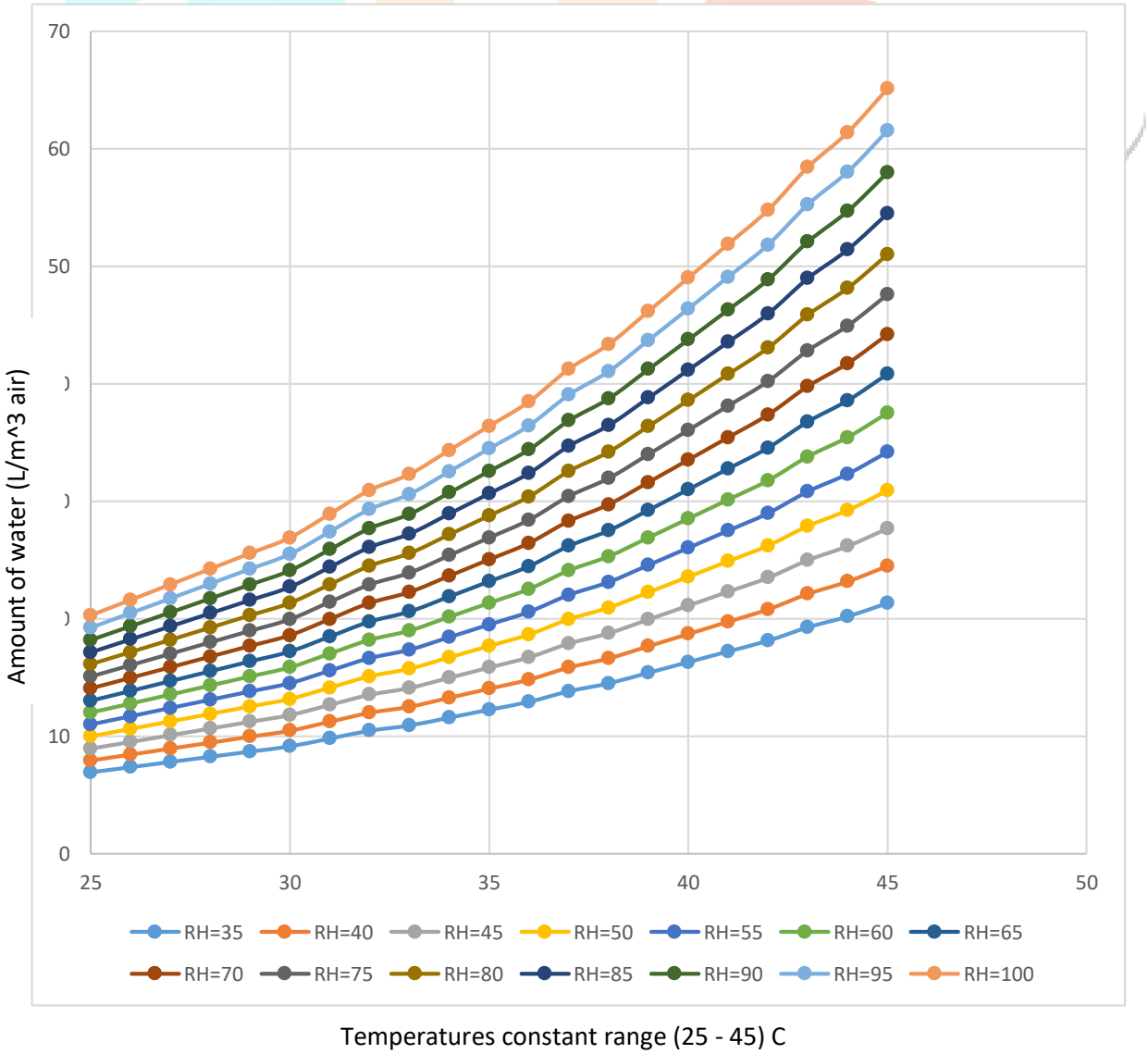

Chart.4 The amount of water present in $1m^3$ in different temperatures and different RH.

6.2.3. Case 3 (Ansys case)

In this case, a numerical simulation using (Ansys 2020R2) is performed to verify the experimental device's results, and the simulation more cases with different conditions to get more results. Thirty-two cases are studied using four inlet velocities (0.25 m/s, 0.5 m/s, 0.75 m/s, 1.2 m/s) with eight values for the inlet temperature which are (288K, 293K, 298K, 303K, 308K, 313K,318K, and 321K) and for relative humidity ranging from 10% to 100% for each case. The results showed that the water production rate increase with a decrease in velocity and increase relative humidity and temperature. The contours of Pressure, Velocity, Temperature, and Humidity will be shown below.

6.2.3.1. Pressure

The pressure decrease of the airflow is roughly the same for all of the cases analysed, according to the numerical results shown in **Figure 13**. This figure shows the static pressure contours in the dehumidification duct, as well as the upstream and downstream flow. The static pressure contours at the duct downstream showed the existence of different pressure regions. However, the static pressure distribution on the cooled face is uniform.

6.2.3.2. Velocity

The effect of velocity on the water production rate was studied. Four different inlet velocities were used, which were 0.25 m/s, 0.5 m/s, 0.75 m/s, and 1.2 m/s, and with different temperatures ranging from 25℃ to 48℃. The water production rate increases when inlet velocity decreases. The contours of velocity magnitude and path lines can be seen in **Figures 14 and 15**.

6.2.3.3. Humidity

The relative humidity contours observed from the numerical results are shown in **Figure 16**. The results show that water production rates increase at maximum humidity in cooled tube regions.

6.2.3.4. Temperature

Figure 17 represents the contour of temperature variations around the cooler. The ISO surface of temperature contours shows the gradient decreased. The temperature distribution in the cold face of each case from the 32 cases is not uniform. The rate of temperature changes throughout the evaporator, which decreased from a maximum of 305K to a minimum of 275K, dependent on inlet velocity, air temperature, and relative humidity.

7. Air-Enhancement

A simulation of air improvement processes is demonstrated so that filters can be installed to purify ambient air and eliminate both contaminants and particulates. The best air filter to install would be a High-Efficiency Particulate Arrester (HEPA) filter.

8. Filtration and TDS testing

The comparisons between the TDS of the water produced by the experimental device, mineral (RO), and the water supplied for houses from the water purification units are given in **Table 2**. The purity of the water produced by air after filtration is good and it can be used by humans since it meets the potable water standards. It can also be treated by adding mineral salts to enhance the health benefits of the users of the water.

Table 2. shown compare between different types of water as TDS testing.

House's water	Mineral water RO	Generation Water from air	Generation Water from the air with filtration & pure
TDS = 591	TDS = 83	TDS = 58	TDS = 48

9. Conclusions and recommendations

Throughout this study, several points can be concluded: First, the possibility to use a device in more applications to remove moisture and to provide air conditioning. Water production depends on the volume of the system and the high levels of humidity, the ability to use the device to produce water in coastal areas, and increasing the inlet velocity of the air decreases the rate of water production rate. In order to extend this study, it is recommended to test the built model with unsteady state conditions, experimentally with accurate instruments, and compare these results with numerous researchers with the same conditions.

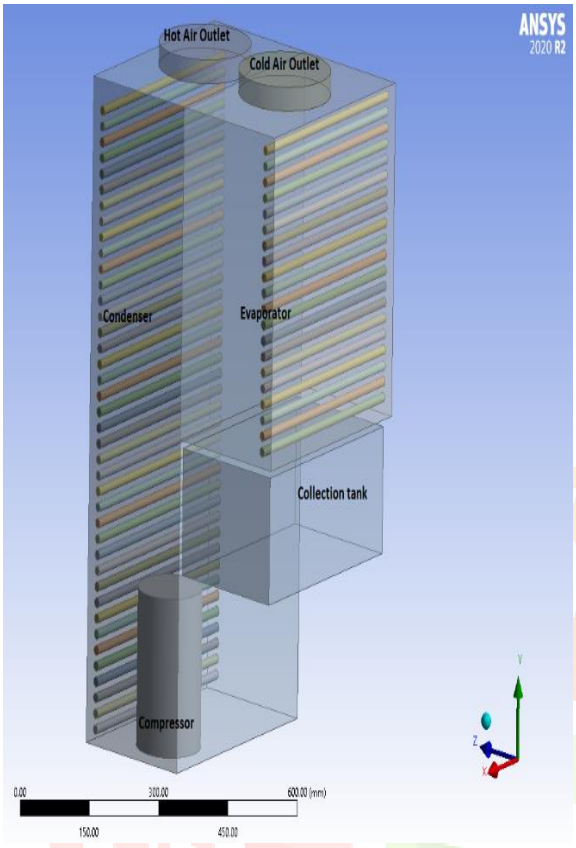

Figure 9. Domain in Design modeler.

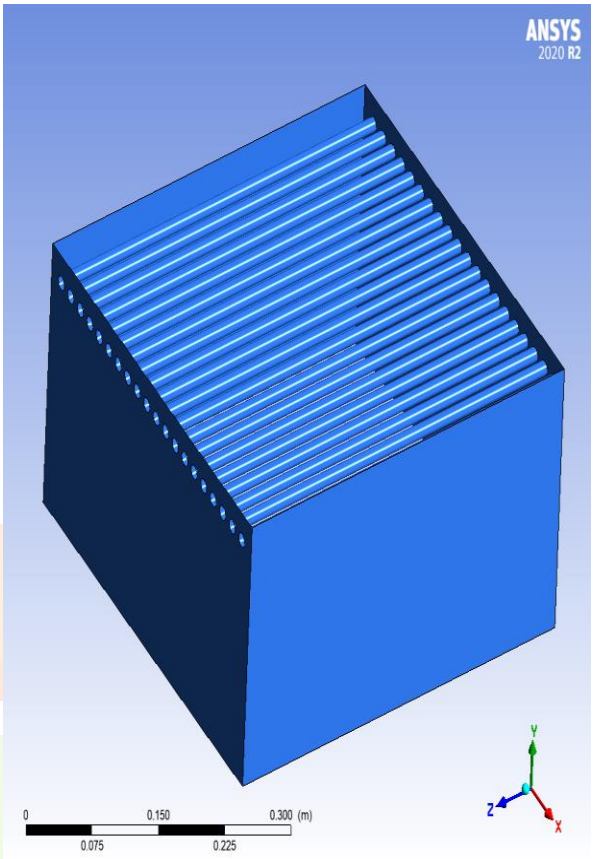

Figure 10. Domain in CFD post.

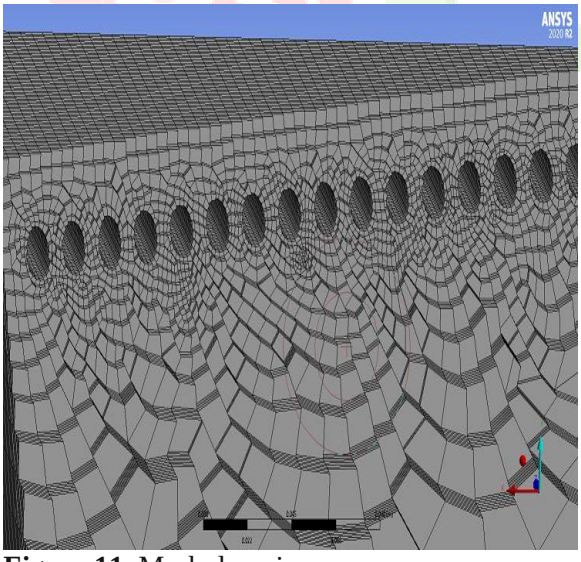

Figure 11. Mesh domain.

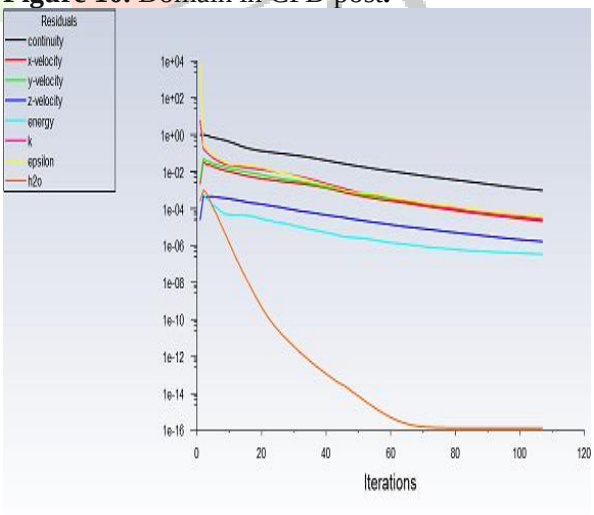

Figure 12. Iteration and convergence of the system.

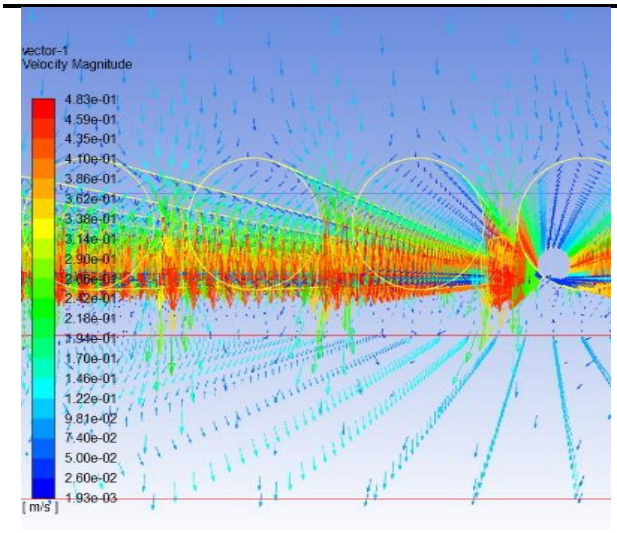

Figure 14. Vector of velocity magnitude.

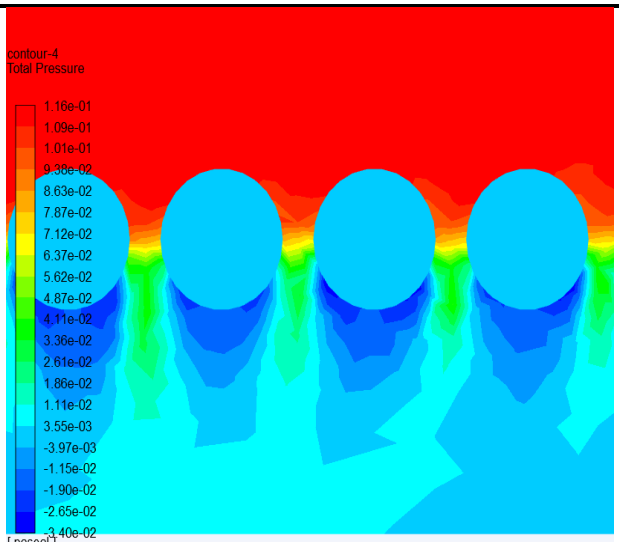

Figure 13. The contour of static pressure.

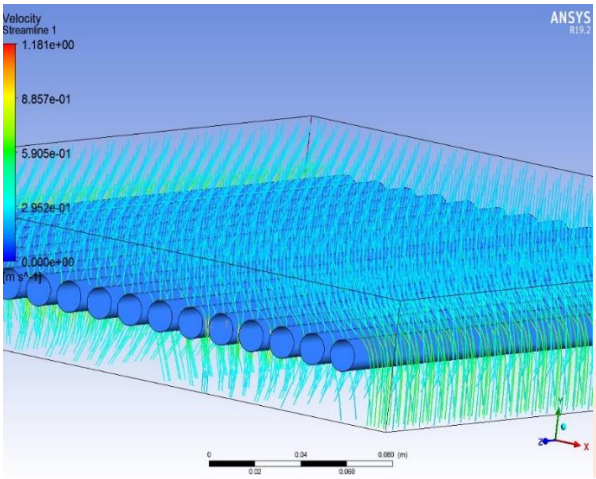

Figure 15. Streamline of velocity magnitude.

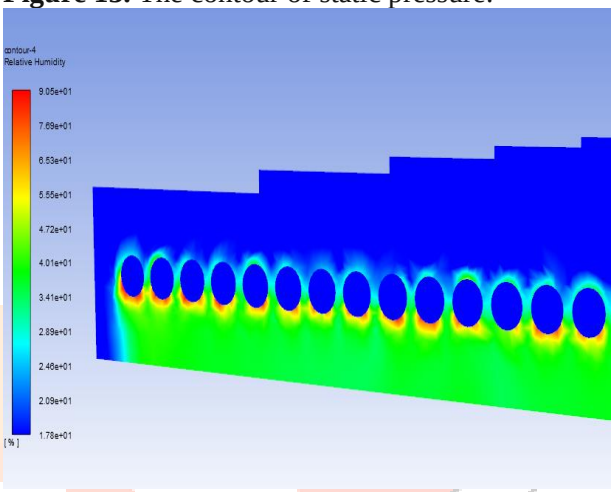

Figure 16. Contours of relative humidity.

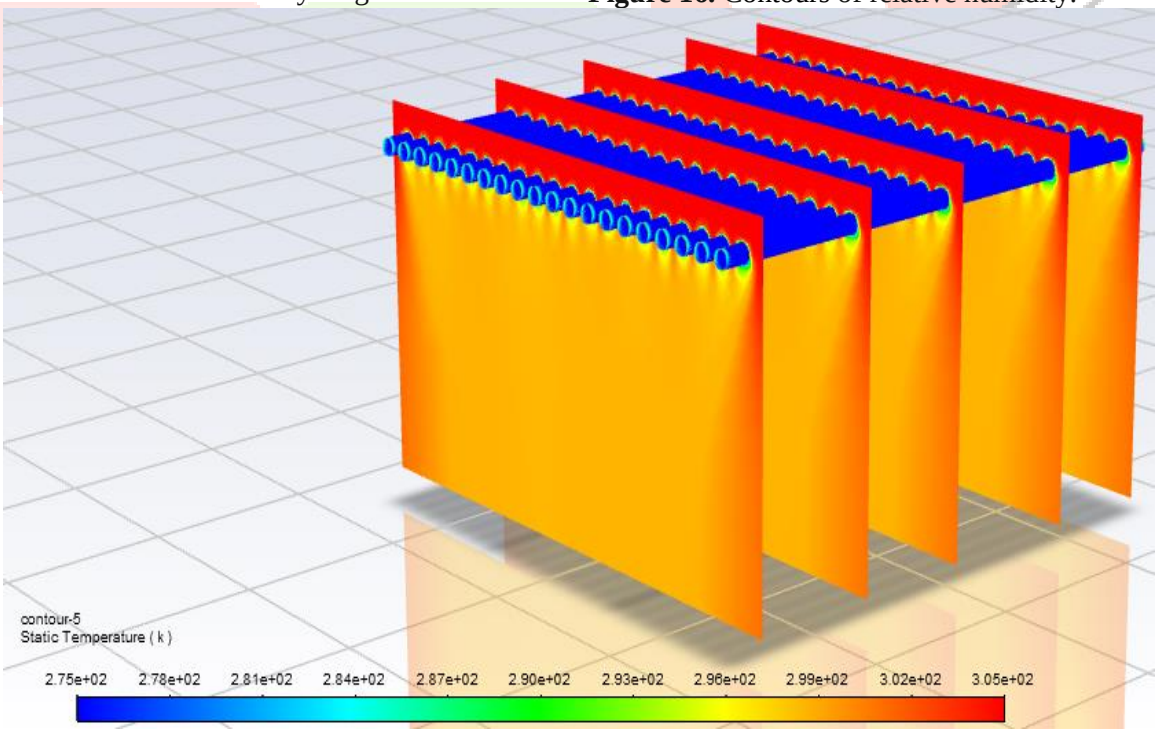

Figure 17. Contours of static temperature.

Nomenclature

WHO	World Health Organization
AC	Air-Conditioning
HVAC	Heating, ventilation, and air conditioning
CFD	Computational Fluid Dynamics.
Exp	Experimental
Num	Numerical
COP	Coefficient of Performance
ρ	Density.
v	Velocity vector.
Γ	Effective exchange coefficient of Ø.
$S_{Ø}$	Source rate per Unit volume.
C	Case
V_s	Supply velocity
P	the pressure of the gas in Pa
V	the volume of the gas in m3
m	the mass of the gas in Kg
R	a constant of proportionality
T	the absolute temperature of the gas in K
P_v	the partial pressure of water vapor in saturated air
P_{sw}	saturated pressure of vapor corresponding to wet bulb temperature from steam table
P_b	barometric pressure
t_w (WBT)	wet bulb temperature
t_d (DBT)	dry bulb temperature

References

[1] Turral Hugh and Jacob Burke and Jean-Marc Faurès, (2011) "Climate Change and Water and Food Security", Food and Agriculture Organization of the United Nations (FAO), ISBN: 9789251067956.

[2] Habeebullah Badr A, (2009) "Potential Use of Evaporator Coils for Water Extraction in Hot and Humid Areas", Elsevier, Desalination, Vol.237, no.1-3, pp.330-45.

[3] Bogardi, Janos J, David Dudgeon, Richard Lawford, Eva Flinkerbusch, Andrea Meyn, Claudia Pahl-Wostl, Konrad Vielhauer, and Charles, (2012) "Water Security for a Planet under Pressure: Interconnected Challenges of a Changing World Call for Sustainable Solutions.", Elsevier, Environmental Sustainability, Vol.4, no. 1, pp.35-43.

[4] Magrini, A, L Cattani, M Cartesegna, (2015) "Production of Water from the Air: The Environmental Sustainability of Air-Conditioning Systems through a More Intelligent Use of Resources. The Advantages of an Integrated System", Elsevier, Energy Procedia, Vol.78, pp.1153-58.

[5] Tripathi Anurag, Samir Tushar, Saurabh Pal, Shoumik Lodh, Shashank Tiwari, (2016) "Atmospheric Water Generator.", International Journal of Enhanced Research in Science, Vol.5, no.4, pp.69-72.

[6] Bagheri Farshid, (2018) "Performance Investigation of Atmospheric Water Harvesting Systems", Elsevier, Water resources and industry, Vol.20, pp.23-28.

[7] M. N. Fares, M. A. Al-Mayyahi, M. M. Rida, and S. E. Najim, "Water Desalination Using a New Humidification-Dehumidification (HDH) Technology," in Journal of Physics: Conference Series, vol. 1279, no. 1, p. 012052: IOP Publishing, 2019.

[8] Ahamed Jamal Uddin, Rahman Saidur, Haji Hassan, (2011) "A Review on Exergy Analysis of Vapor Compression Refrigeration System," Elsevier, Renewable and Sustainable Energy Reviews, Vol.15, no. 3, pp.1593-600.

[9] Yapıcı, R, HK Ersoy, A Aktoprakoğlu, HS Halkacı, (2008) "Experimental Determination of the Optimum Performance of Ejector Refrigeration System Depending on Ejector Area Ratio" International journal of refrigeration Yiğit, Vol.31, no. 7, pp.1183-89.

[10] H. S. Mohammed, E. A. Khazal, and H. S. Sultan, "Studying the Effect of Perforation Parameters on Vertical Well Performance,", Basrah Journal for Engineering Sciences, vol. 20, no. 2, 2020.

[11] Mohammed Alsheekh, " Numerical and Experimental Study of The Best Air Conditioning System of a Large Athletic Hall (Wrestling Hall)" M.Sc. Thesis Mechanical Engineering, University of Basrah,2015.

[12] Haywood and Richard Wilson, (1990) "Thermodynamic Tables in Si (Metric) Units" Cambridge University Press, ISBN 0521386934.

Mohammed Alsheekh, received a B.Sc. degree in General Mechanical Engineering, an M.Sc. degree, and a Ph.D. in Thermo-Mechanical Engineering from the University of Basra, College of Engineering, Basra, Iraq, in 2000 and 2022. I am currently working as a mechanical engineering researcher. *https://orcid.org/0000-0002-6086-3962*

Hussein S. Sultan, Received his degree in Mechanical Engineering, BSc. In 1999, M. Sc. in 2001, and Ph.D. in Mechanical Engineering (Thermal-Mechanics) from Basra University/Engineering College in 2011. currently, a Boss of the Oil Engineering Department and Associate Professor at the Mechanical Engineering Department, Basra University, teaches and supervises undergraduate M. Sc. and Ph.D. students.